J Geophys (1986) 60:157–166

Journal of Geophysics

Cross spectral analysis of Swabian Jura (SW Germany) three-component microearthquake recordings

F. Scherbaum and J. Wendler

Institut für Geophysik der Universität Stuttgart, Richard-Wagner-Str. 44, D-7000 Stuttgart 1, Federal Republic of Germany

Abstract. Similar three-component microearthquake records have been observed in the Swabian Jura (SW Germany) seismic zone for different source-receiver geometries. This data set is used to study the resolution power of cross spectral analysis techniques for the estimation of relative differential times as well as the applicability to velocity monitoring. The differential times are estimated in the frequency domain by assuming a linear-phase cross spectrum with the slope indicating the individual time difference. All earthquakes have been relocated with respect to a master event, using the relative *P* and *S* delay times from the cross spectral analysis as a measure of source mislocation. The overall location error is strongly dependent on the inital distance between master and studied event. For earthquakes initially located farther apart than approximately 1.5 km, the relocalization result in terms of total location error was poorer, whereas for events initially located closer than 1 km the precision of the relocalization was improved. The remaining residuals are of the order of 10 ms, which is approximately 3 times the digitization interval.

In order to test the applicability of cross spectral analysis to velocity monitoring, synthetic data were used to model the influences of noise and source time function differences. The effect of additive white noise seems to be acceptable in cases where the S/N ratio is sufficiently high. Small changes in the shape of the source time function, however, were found to be of great influence to the differential time estimates. Variation of rise, sustain and decay times, which were negligible in the coherence spectrum, spuriously introduced phase differences which, in terms of delay times, easily reach the magnitude of the digitization interval. Thus, velocity monitoring using cross spectral analysis techniques seems to depend strongly on the equality – in contrast to similarity – of the source time functions of the events which are compared. The coherence spectrum is not a sufficient measure to detect all the significant differences.

Key words: Cross spectral analysis – Similar earthquakes – Earthquake doublets – Swabian Jura earthquake zone – Hypocenter relocation

Introduction

The application of cross spectral analysis (CSA) techniques has been recently demonstrated to provide relative travel-time differences between the two events of an earthquake doublet with extraordinarily high accuracy (Poupinet et al., 1984; Frechet, 1985). If the two events are generated at essentially the same source location, this information can be used to resolve velocity changes in the crust (Poupinet et al., 1984; Fremont, 1984; Ito, 1985; Poupinet et al., 1985). For similar earthquakes, which do not necessarily have to originate at the *same* location, the information on the time differences can be exploited for precise relative relocation, thus offering a powerful method to investigate the fine structures of source regions (e.g. Evernden, 1969; Dewey, 1979; Ito, 1985). In the following, the term doublet is used for earthquakes occurring at an identical location, whereas similar earthquake is used as a more general term to describe events with waveform likeness.

For the Swabian Jura (SW Germany) earthquake zone, the observation of similar microearthquake recordings, including doublets from a relatively large area – approximately 10 km in diameter – (Scherbaum and Stoll, 1985; Scherbaum, 1986; Langer, 1986), offers the opportunity of studying the applicability range of the cross spectral analysis method. The purpose of the present paper is to investigate the resolution power of the CSA method using three-component records for relocation purposes as well as for velocity monitoring. Synthetic seismograms were used to test the influence of different source time signals on the resolution of onset times. Additionally, the influence of the source distances and the influence of noise will be demonstrated.

Figure 1 shows the location of the Swabian Jura earthquake zone within the Federal Republic of Germany. The local digital seismic network has been in operation since 1976. The area of investigation has shown three major earthquake sequences with main shock magnitudes of the order of MWA = 5.5–6.0 (MWA = Local Magnitude) since the beginning of this century. The last major event occurred in 1978 (MWA = 5.7) and was followed by a large number of aftershocks (Haessler et al., 1980; Turnovsky and Schneider, 1982; Scherbaum and Stoll, 1983). In 1982, the network was expanded to seven four-component stations, unified in its instrumental characteristics and rearranged to its present position (Table 1). The dataset used in this study consists of the microearthquake recordings obtained between October 1982 and the present. This time period is characterized by a comparably very low seismic activity. Only some 30 events have been detected. For the present study however, only events which were recorded by at least three stations were analysed. Thus, the dataset consists of six events. Table 2 lists the events which were used for the

Offprint requests to: F. Scherbaum

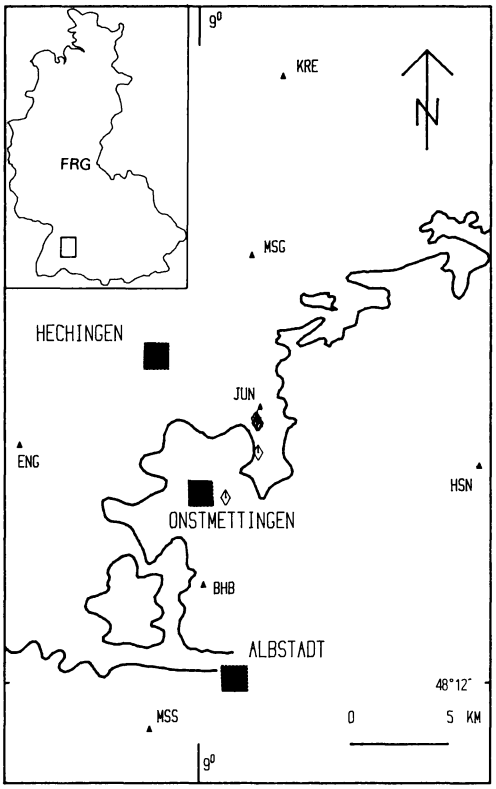

Fig. 1. Geographical location of the Swabian Jura, SW Germany, earthquake zone. The *inset* shows the position of the area under study with respect ot the Federal Republic of Germany. The *solid triangles* indicate the recording stations of the Swabian Jura seismic network. *Diamonds* show the relocations of the earthquakes under study. The *solid line* indicates the outcrop of the Upper Jurassic limestone which is the most prominent topographic feature in the Swabian Jura region

present analysis. The locations and source parameters were taken from Langer (1986). As far as fault-plane solutions could be obtained, the focal mechanisms are consistent with a NNE-SSW-striking, left-lateral strike-slip fault (Langer, 1986). The distribution of epicenters is given in Fig. 2, in addition to the positions of the individual recording stations.

The cross spectral analysis method

The cross spectral analysis technique as applied by Poupinet et al. (1984) and Ito (1985) is based on the estimation of the travel-time differences in the frequency domain from the phase of the corresponding cross spectrum.

Provided that two time signals of identical shape s_1 and s_2 and a magnitude difference c are observed at a time difference τ, that is

$$s_2(t) = c \cdot s_1(t-\tau),$$

the corresponding Fourier spectra $S_1(\omega)$ and $S_2(\omega)$ are given by:

$$S_1(\omega) = |S_1(\omega)| \cdot e^{i\phi_1}, \tag{1}$$

$$S_2(\omega) = c \cdot |S_1(\omega)| \cdot e^{i\phi_2} \tag{2}$$

$$= c \cdot |S_1(\omega)| \cdot e^{i(\phi_1 - \omega t)} \quad \text{(shifting theorem)}. \tag{3}$$

The corresponding cross spectrum is defined as (*denoting complex conjugate):

Table 1. Main characteristics of the Swabian Jura local network

Station coordinates

Station	Longitude E	Latitude N	Altitude (m)
BHB	9° 00′ 07″	48° 14′ 50″	890
ENG	8° 52′ 28″	48° 18′ 38″	537
HSN	9° 11′ 38″	48° 18′ 15″	710
JUN	9° 02′ 27″	48° 19′ 49″	600
KRE	9° 03′ 22″	48° 28′ 55″	458
MSG	9° 02′ 04″	48° 23′ 57″	475
MSS	8° 57′ 56″	48° 10′ 47″	915

Instrumental characteristics

Recording method	Digital PCM code on 1/4″ magnetic tape			
Seismometer	Channel 1 (Z) Strobach	Channel 2 (N) Willmore MK III	Channel 3 (E) Willmore MK III	Channel 4 (E/N) Sundstrand Q-Flex
Eigen-frequency (HZ)	0.66	0.66	0.66	800
Sensor type	Dis-placement	Velocity	Velocity	Acceleration

A/D conversion 12 bit, 72 dB

$$C(\omega) = |C(\omega)| \cdot e^{i\phi_c} \tag{4}$$

$$= S_1(\omega) \cdot S_2(\omega)^* \tag{5}$$

$$= c \cdot |S_1(\omega)| \cdot |S_1(\omega)| \cdot e^{i\phi_1} \cdot e^{-i(\phi_1 - \omega\tau)} \tag{6}$$

$$= c \cdot |S_1(\omega)|^2 \cdot e^{i\omega\tau}. \tag{7}$$

As can be seen from Eq. (7), in the case of identical signals, the cross spectrum is linear phase with the differential time τ being the slope of the phase spectrum, that is:

$$\Phi_c = \omega\tau. \tag{8}$$

In the case of additive uncorrelated noise, the slope of the phase is assumed not to be affected (Ito, 1985).

The likeness of real data, however, is never perfect. Similarity might be restricted to particular frequency bands or limited by noise. Thus, the degree of uniformity between the different signals has to be taken into account in the analysis. A well-established measure for the amount of association is given by the coherence spectrum COH (ω) (Kanasewich, 1981):

$$\mathrm{COH}(\omega) = \frac{\mathrm{CS}(\omega)^2}{\mathrm{PS}_1(\omega)^* \mathrm{PS}_2(\omega)}, \tag{9}$$

$\mathrm{CS}(\omega)$ = smoothed cross spectrum C (ω),
$\mathrm{PS}_1(\omega)$ = smoothed power spectrum of signal 1,
$\mathrm{PS}_2(\omega)$ = smoothed power spectrum of signal 2.

Smoothing is required, otherwise the coherence will always be unity regardless of the nature of the process (Kanasewich, 1981).

The data analysis

The data analysis has been performed following the moving window procedure of Poupinet et al. (1984). In the first

Table 2. Earthquakes under study from the observation period October 1982–July 1985. Only events which have been recorded by at least three stations are displayed. Source parameters and locations from Langer (1986)

No.	Date	Time	Lat (°N)	Lon (°E)	Z (km)	MWA	M_0 (Nm)
03	1982 Nov 28	04:34	48° 18.2′	09° 02.2′	07.0	3.8	8.5×10^{13}
16	1983 Sep 11	11:48	48° 19.2′	09° 02.4′	05.5	3.6	4.0×10^{13}
18	1983 Sep 14	10:52	48° 18.9′	09° 02.4′	05.0	1.9	7.1×10^{11}
19	1983 Sep 14	18:25	48° 19.1′	09° 02.4′	05.5	2.3	1.9×10^{12}
20	1983 Sep 15	06:26	48° 19.1′	09° 02.4′	05.0	3.1	1.6×10^{13}
25	1984 Jan 03	15:28	48° 15.2′	09° 02.7′	09.4	2.5	2.8×10^{12}

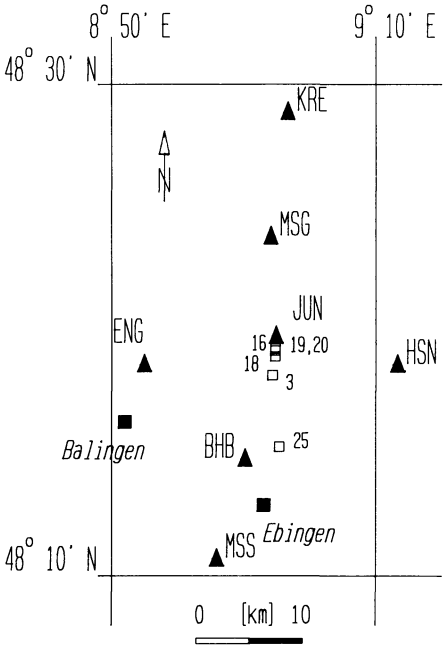

Fig. 2. Distribution of epicenters before relocations (*open squares*) of the earthquakes used for the cross spectral analysis. The *numbers* denote event numbers referred to in the text. The *solid triangles* indicate the recording stations of the Swabian Jura seismic network

step, the two records were aligned as closely as possible in order to avoid constant phase shifts in the cross spectra (e.g. Fig. 3a and b). A window of 0.96 s duration (256 samples), tapered with a cosine bell affecting 50% of the total window length, was moved along the seismograms in steps of 0.24 s (64 samples). This particular parameter set was obtained to yield an optimum time resolution for synthetic seismograms calculated for structural models resembling the geological situation in the studies area (Scherbaum, 1986) and sampled with the actual digitization frequency of 267 Hz.

For each time step, the cross spectrum, Eq. (5), and the coherence, Eq. (9), were calculated for the analysis window. The spectral smoothing required for the estimation of the coherence was carried out by weighted averaging over five neighbouring spectral estimates. The coherence has been scaled to give unity for identical, time-shifted signals. In Fig. 3d and e for example, the modulus of the cross spectrum and the coherence spectrum, respectively, for the first window of Fig. 3a and b are displayed. Finally, the relative time difference for an individual window was estimated by fitting a straight line to the slope of the cross phase spectrum according to Eq. (8). Following Poupinet et al. (1984), the phase of the cross spectrum was weighted for the regression analysis. The product of the cross spectrum and the coherence was chosen as a weighting factor in order to concentrate on the strongest and most coherent signal components (Fig. 3e). Frequencies above the passband of the recording system (0.5–50 Hz) as well as contributions from spectral components with a weighting factor below a certain level were completely ignoured (cf. Fig. 3f). The cutoff level for the weighting factor was chosen arbitrarily to be 0.4 in order to limit the regression analysis to that part of the phase spectra where the slope seemed to be essentially linear. The dotted line in the phase plots (e.g. Fig. 3f) gives the phase angle corresponding to a differential time of one sampling interval (3.75 ms). For each time step, the delay time was estimated following the same procedure and displayed as a function of lapse time along the seismogram (e.g. Fig. 3c).

Time differences from CSA were estimated for all the records with suffcient quality for the vertical (displacement) and the two horizontal components (velocity). The strong motion channel (acceleration) was not considered in the present analysis. Event 20 (1983 Sep 15, 06:26) was chosen as the master event, since it has been recorded and located by six out of seven stations.

In Figs. 3–5, the results of the CSA differential time measurements for events 19 and 20 at the recording station ENG (Engstlatt) are displayed. Cross amplitude spectra, coherences and cross phase spectra are displayed for those time windows containing either P_g or S_g. As a consequence of the small hypocentral distances (Fig. 2), these phases are in general easily identified in the observed seismograms. Figure 3a–c shows the aligned vertical seismogram components (Fig. 3a and b) together with the corresponding delay times as a function of lapse time along the seismogram (Fig. 3c). The squares in Fig. 3c indicate the centre times of the individual window positions (e.g. first window at 0.48 s). In Fig. 3d–f the cross amplitude spectrum, coherence and phase of the cross spectrum, respectively, for the first window – which is assumed to contain the P pulse – are displayed. Figures 4 and 5 show the result of the CSA analysis for the two horizontal components. For the display of the cross spectrum, coherence and phase of the cross spectrum for this trace, window 8 was assumed to contain the direct S pulse (cf. Figs. 4a and 5a). All the phase plots exhibit as sufficient linear slope in that frequency band where the phase weighting factor (cross spectrum × coherence) is above the cutoff level. The coherence for events 19 and 20 is close to one for all frequencies, which might indicate that these earthquakes are doublets.

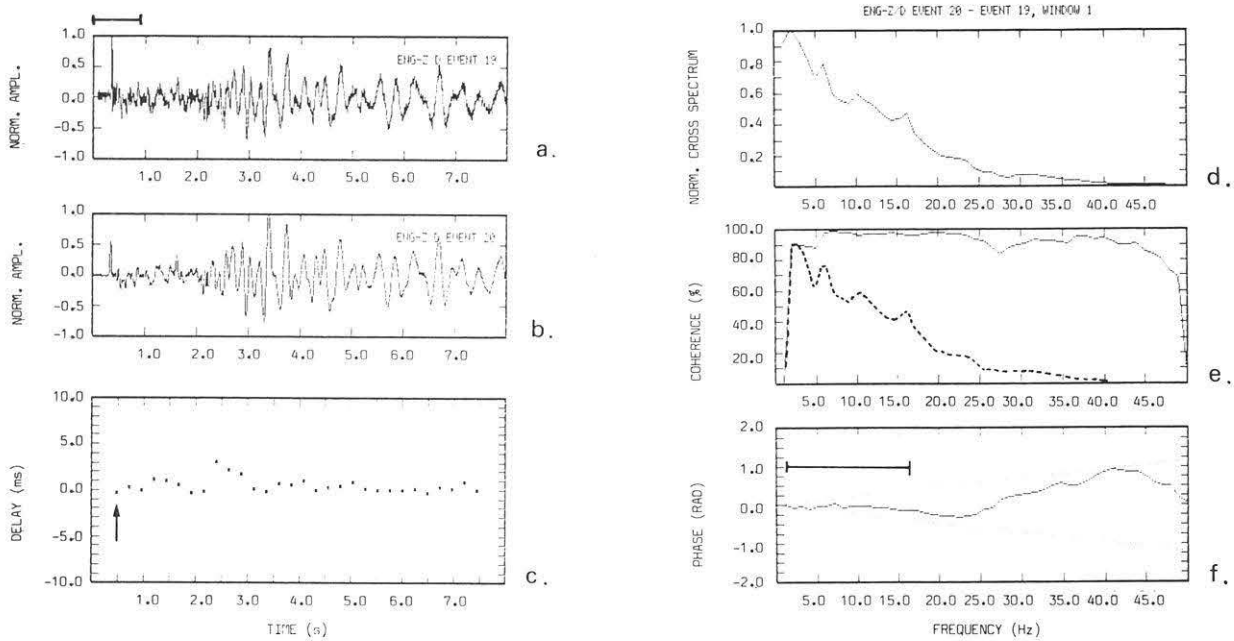

Fig. 3a–f. Cross spectral analysis of event 19 as compared with event 20. **a** and **b** show the aligned vertical component seismograms, **c** gives the delay times as a function of lapse time and **d** shows the cross amplitude spectrum for the window containing the *P* pulses. The window centre time and the corresponding window margins are indicated in Fig. 3c (*arrow*) and above Fig. 3a, respectively. **e** shows the coherence (*solid line*) and the weighting factor for the regression analysis (*dashed line*). **f** displays the corresponding phase spectrum. The frequency band used for regression analysis is indicated by the *horizontal bar*. The *dotted line* corresponds to the delay time equal to the sampling interval. Recording site is ENG

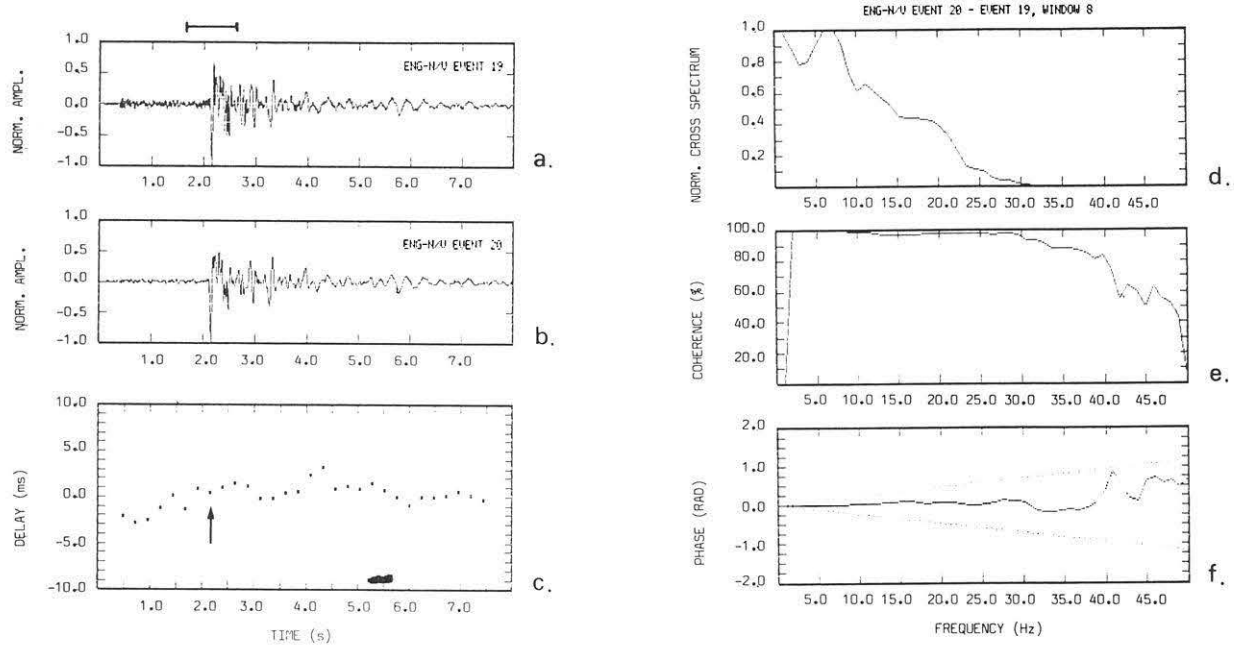

Fig. 4a–f. Cross spectral analysis of event 19 as compared with event 20. **a** and **b** show the aligned N–S component seismograms, **c** gives the delay times as a function of lapse time and **d** shows the cross amplitude spectrum for the window containing the *S* pulses. The window centre time and the corresponding window margins are indicated in Fig. 4c (*arrow*) and above Fig. 4a, respectively. The coherence is given in **e**. The corresponding phase spectrum is displayed in **f**. The *dotted line* corresponds to the delay time equal to the sampling interval. Recording site is ENG

The delay times (differential times) for all traces as a function of lapse time do not show oscillations. Thus, velocity changes between the occurrence time of these two events are not observable from this analysis.

Figures 6–8 give the seismograms, delay times, cross spectra, coherences and phase plots for event 16 as compared to the master event, 20. The similarity of the dominant waveforms in terms of coherence (Figs. 6e, 7e, 8e) is still sufficient in the frequency band defined by the cutoff level of the weighting function, although it is clearly less

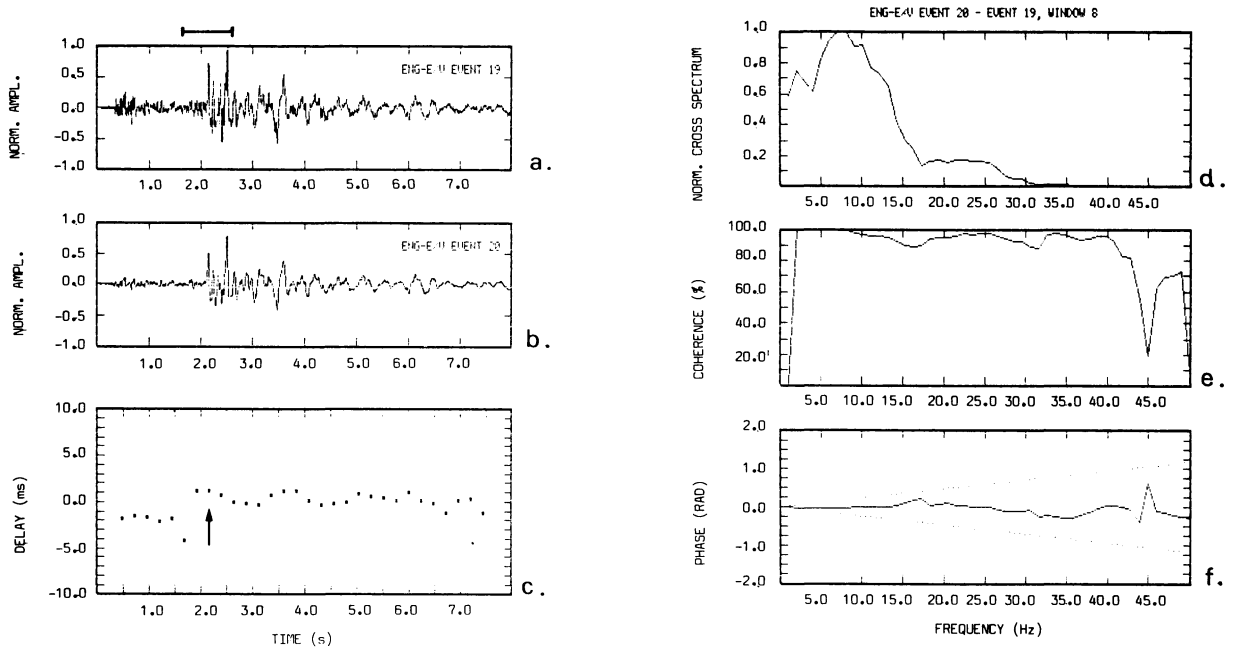

Fig. 5a–f. Cross spectral analysis of the E–W component seismograms for event 19 as compared with event 20. Recording site is ENG. For explanations, see Figs. 3 and 4

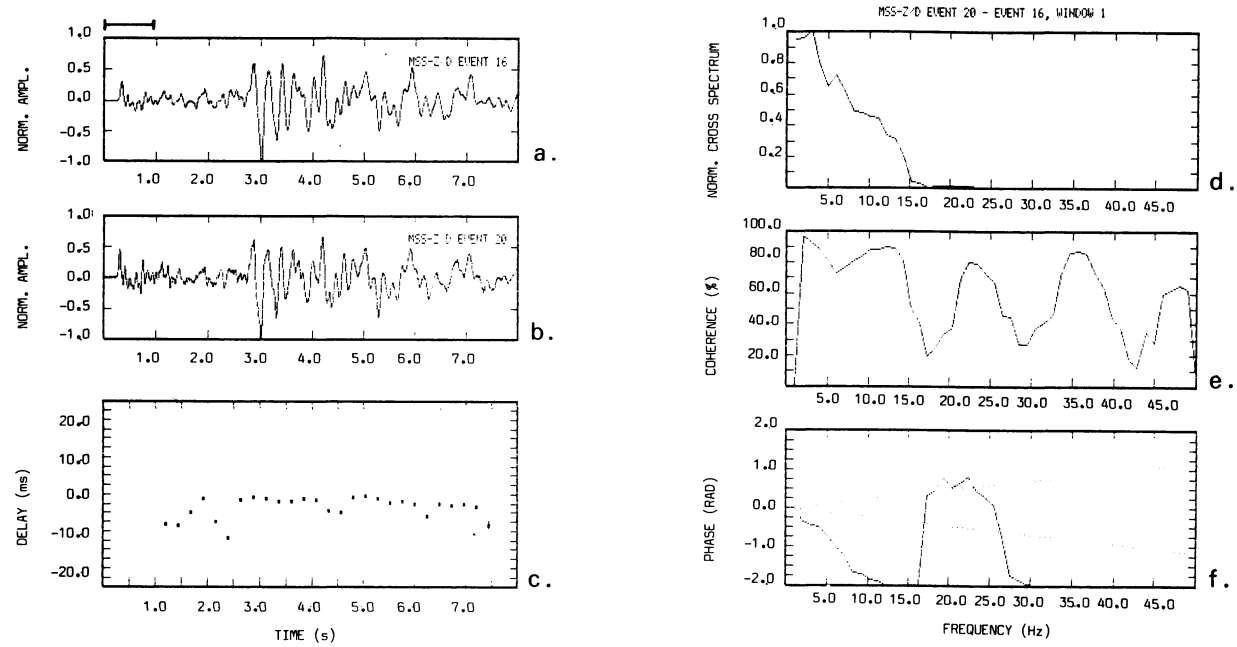

Fig. 6a–f. Cross spectral analysis of the vertical component seismograms for event 16 as compared with event 20. Recording site is MSS. For explanations, see Figs. 3 and 4. Differential time for the *P* pulses outside the plotting range

than for events 19 and 20. Additionally, the delay times vary more strongly as a function of lapse time. This might be due to a certain amount of noise in the records of event 20 at this station as well as a consequence of hypocentral differences.

All events were processed in a similar way in order to obtain the delay times as compared to the master event. For each two seismograms to be compared, the delay times for the windows containing the P_g and S_g arrivals were chosen from the individual delay time versus lapse time plots (e.g. Fig. 3c). Finally, these values were corrected for the time differences introduced due to the different alignment of the individual traces in the first step of the analysis. The results are given in Table 3.

Relocation of hypocenters

The most obvious reason for the delay times to show differences for the individual stations is a difference in the location of the events under comparison. For this reason, a

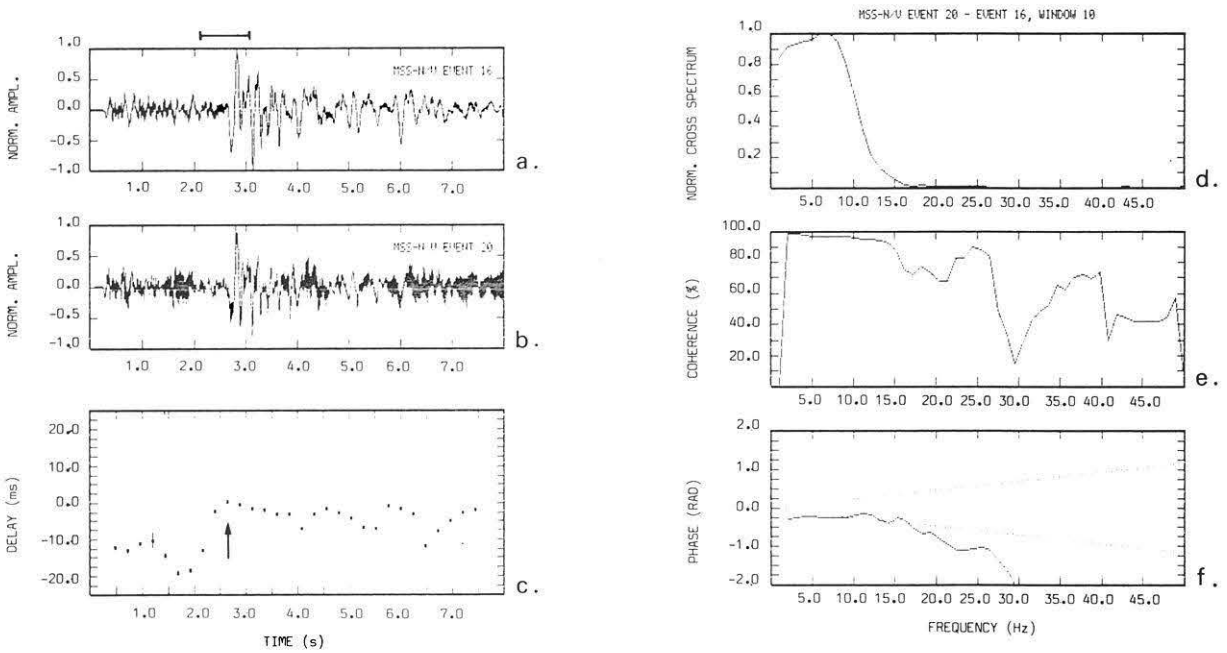

Fig. 7a–f. Cross spectral analysis of the N–S component seismograms for event 16 as compared with event 20. Recording site is MSS. For explanations, see Figs. 3 and 4

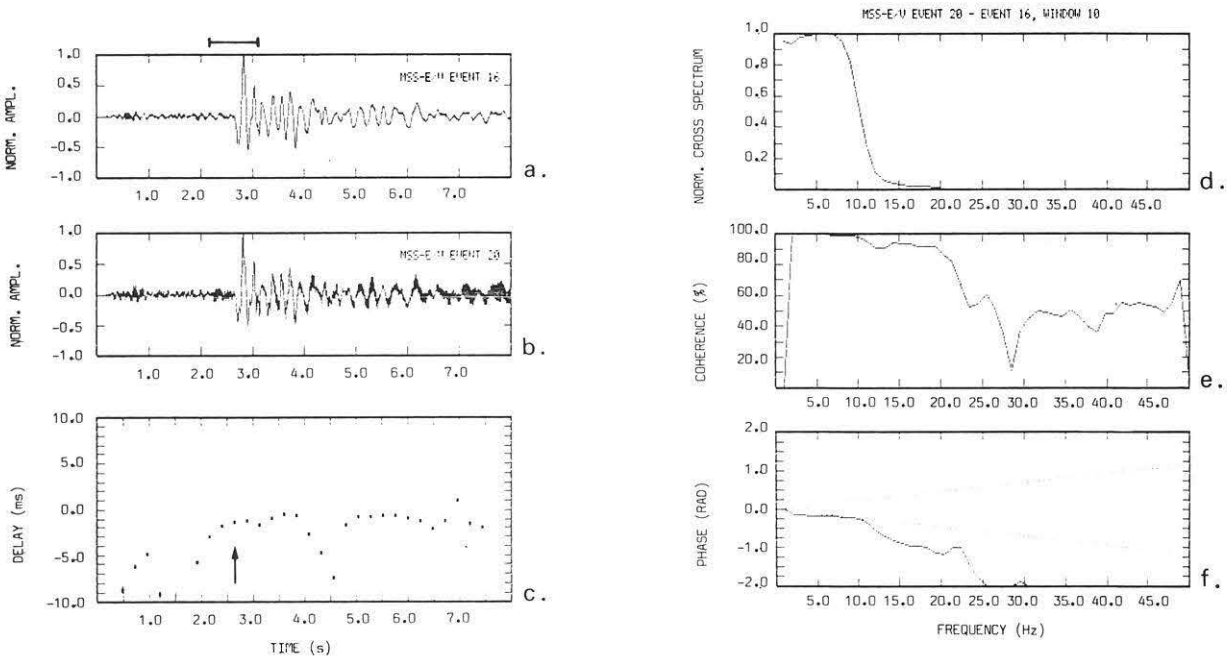

Fig. 8a–f. Cross spectral analysis of the E–W component seismograms for event 16 as compared with event 20. Recording site is MSS. For explanations, see Figs. 3 and 4

relocalization has been performed using a master event technique (e.g. Evernden, 1969; Dewey, 1979; Ito, 1985). For this purpose we calculated new individual arrival times using

$$P_{ik} = P_{mk} - \tau_{pik}$$
$$S_{ik} = S_{mk} - \bar{\tau}_{sik} \qquad (10)$$

Here, P_{ik} and S_{ik} are the new P and S onset times, respectively, for event i at station k. The index m denotes the master event index. τ_{pik} is the P-wave differential time obtained from the vertical component, $\bar{\tau}_{sik}$ the averaged S-wave differential time obtained from the two horizontal components if possible. The localizations were obtained using a modified version of HYPO71 (Gelbke, 1977; Lee and Lahr, 1972).

As can be seen from Table 3, there are large differences in the delay times for the S phases estimated for different components, especially, if the event was located at some distance from the master event (e.g. event 25). Only for event 19, as compared with the master event, are the differ-

Table 3. Relative differential times (in ms) for the individual components. For the *Z* component, the differential times of the windows containing the *P* pulses are listed. For the N and E components, differential times for the *S*-pulse windows are given. All delay times are corrected for the different alignment of the individual traces prior to the cross spectral calculations

No.	Date	Time		Relative delay times in ms						
				BHB	ENG	HSN	JUN	KRE	MSG	MSS
03	1982 Nov 28	04:34	*Z*	−94.3		–			−58.5	−85.8
03	1982 Nov 28	04:34	N	28.0		−128.1			−258.2	61.5
03	1982 Nov 28	04:34	E	−12.8		–			−364.7	60.2
16	1983 Sep 11	11:48	*Z*	−44.9		26.1			−69.7	−31.5
16	1983 Sep 11	11:48	N	−6.4		0.0			−84.8	0.0
16	1983 Sep 11	11:48	E	−16.6		0.0			−96.0	1.0
18	1983 Sep 14	10:52	*Z*	−215.2		–			−56.8	
18	1983 Sep 14	10:52	N	−176.2		−191.0			−172.9	
18	1983 Sep 14	10:52	E	−185.9		−206.3			−81.7	
19	1983 Sep 14	18:25	*Z*	62.1	78.4	–		−205.8	−18.8	
19	1983 Sep 14	18:25	N	−60.8	79.3	–		–	−17.3	
19	1983 Sep 14	18:25	E	−62.1	79.9	26.9		−202.9	−20.7	
20	1983 Sep 15	06:26		Master event						
25	1984 Jan 03	15:28	*Z*	37.0						−11.2
25	1984 Jan 03	15:28	N	413.9	154.8					960.7
25	1984 Jan 03	15:28	E	362.2	139.2					896.0

Table 4. Relocation vector (*X*, *Y*, *Z* in m) pointing from the original location to the hypocenter from the relocalization

No.	Date	Time	Relocation vector in m		
			X	*Y*	*Z*
03	1982 Nov 28	04:34	304	−33	2,730
16	1983 Sep 11	11:48	221	−95	−830
18	1983 Sep 14	10:52	161	−75	−900
19	1983 Sep 14	18:25	−32	86	−130
20	1983 Sep 15	06:26	Master event		
25	1984 Jan 03	15:28	−139	3,979	−1,190

ences in delay times for the two horizontal components below the duration of the digitization interval. Therefore, the average *S* delay times used for the relocations of events which were observed under different back azimuths might be in error. On the other hand, from data quality criteria, no preference could be given to any of the single components.

The differences between relocations and original locations are given in Table 4. The shift of the epicenters as a result of the relocalization is shown in Fig. 9. The amount of shift is strongly related to the original hypocentral distance to the master event. The closest events were shifted by approximately 100 m, whereas the farthest event was moved by the relocalization by approximately 4 km. In order to measure the improvement of the relocalization, the total location error for the original location and for the relocalization was calculated (Table 5). This quantity has been defined as the arithmetic mean of the standard deviations for the individual coordinate axes in the location procedure. It can be viewed as a measure of the size of the volume where the true hypocentre is located with a specific probability. In Fig. 10 the ratios of the total loca-

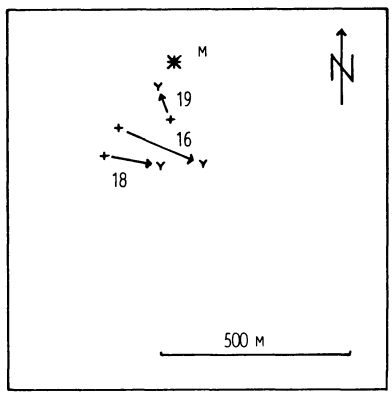

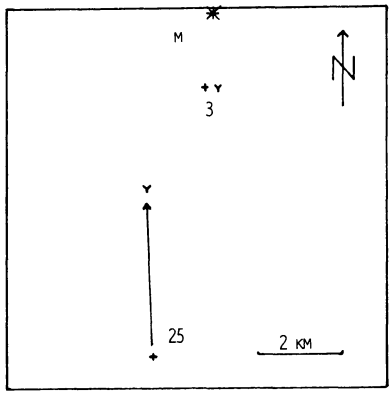

Fig. 9a and b. Difference vectors for the relocated epicenters as compared to the original locations. **a** shows the results for the events with small difference, whereas in **b** the difference vectors for the events with large epicentral shifts due to the relocalization are displayed. Old epicentres are denoted by +, relocated epicentres by y

Table 5. Location errors for the original locations and relocations together with the error ratio. Location error was defined as the arithmetic mean of the localization standard deviation for the individual coordinate axes

No.	Date	Time	Location error in km		
			Original location	Relocation	Ratio
03	1982 Nov 28	04:34	0.316	1.451	0.218
16	1983 Sep 11	11:48	0.316	0.312	1.013
18	1983 Sep 14	10:52	0.106	0.045	2.356
19	1983 Sep 14	18:25	0.208	0.101	2.059
20	1983 Sep 15	06:26	0.316		
25	1984 Jan 03	15:28	0.277	4.295	0.064

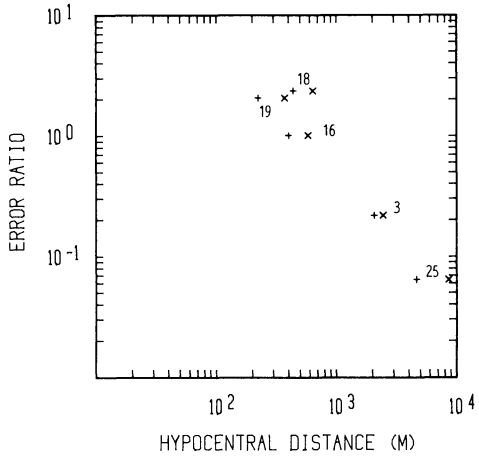

Fig. 10. Ratio of total location errors before and after relocation as a function of the individual event – master event distance. The x refer to the original distance, the + to the relocated distances. For the explanation of the total location error, see text

tion errors for the original localizations and the relocalizations are given as a function of the hypocentral distances to the master event. Only for events as close as 0.5 km from the master event could an improvement of the localization be obtained by the CSA method. This result is in agreement with the observation of increasing standard deviations with increasing distances from the master event shown by Ito (1985).

The influence of errors

A) Instrumental errors

Systematic time shifts for the samples of neighbouring data channels are introduced during recording due to a multiplexed analog to digital conversion. Since this time difference is the same for the same channels at different stations, it has not been considered further.

After digitization, the time code is added to the data frame through a transmitter-synchronized time signal. The maximum tolerance is reported to be 1 ms (Lennartz electronic, personal communication, 1986). Since the data are digitized at the site, additional errors such as tape speed variations, telephone line delays, etc., are of no concern for the present analysis. Furthermore, errors due to instrumental differences are below the instrumental tolerance since all the recording systems are the same.

B) The influence of source pulse differences

In order to investigate the amount of error which might be introduced by source pulse differences, we performed the CSA method on a number of synthetic data with different source time functions. The geometry was chosen to resemble the actual situation in the present study using a well-established crustal model for the Swabian Jura earthquake zone (e.g. Langer, 1986). The seismograms were cal-

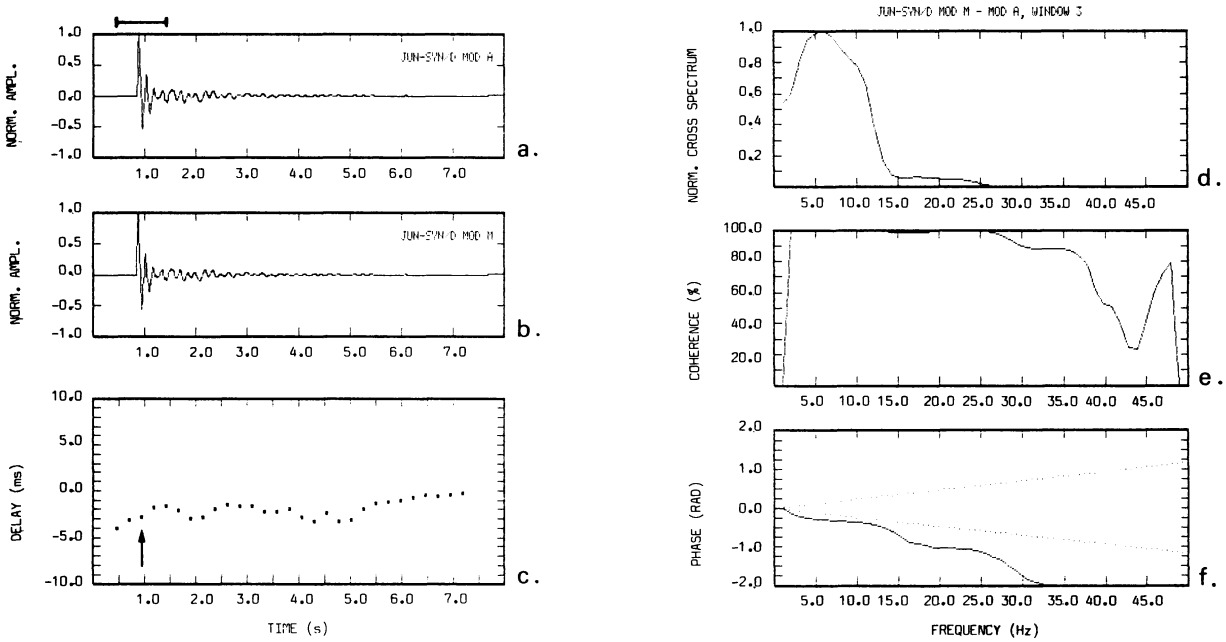

Fig. 11a–f. Cross spectral analysis of noise-free synthetic seismograms from the same source location, but different source time functions. **a** and **b** show the aligned *SH* seismograms, **c** gives the differential times versus lapse time. **d** shows the cross amplitude spectrum for the window containing the *S* pulses. **e** and **f** give the corresponding coherence and cross phase spectrum, respectively. The *dotted line* in the phase plot corresponds to the delay time equal to the sampling interval

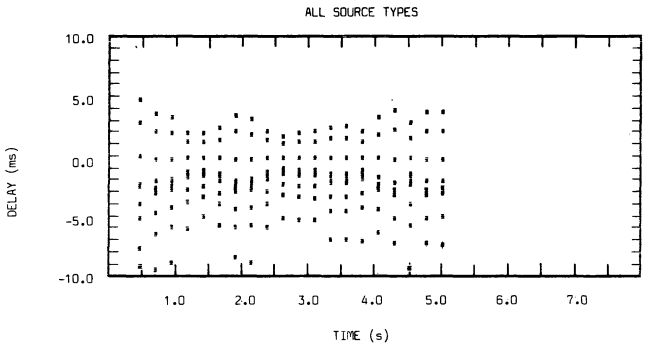

Fig. 12. Overall scatter of spurious times introduced by differences in the source functions. The amount of variation is explained in the text

culated for plane *SH* waves propagating in a stack of horizontal layers using the Haskell (1960) method. The source time functions consisted of trapezoidal pulses, defined by the three parameters: rise, sustain and decay time. These parameters were chosen for the synthetic master event to be 0.01, 0.02, 0.01 s in order to obtain a frequency content comparable to the observed signals. By variation of the individual source time parameters between 0.0 and 0.03 s with steps of 0.01 s, a number of slightly different individual events were simulated. The source locations were held fixed. An example is given in Fig. 11. As can be seen, the coherence of the different seismograms is close to one, not showing any significant difference in the signal shape. However, due to the phase differences of the source pulses, a spurious time difference is introduced (Fig. 11c and f). The amount of error introduced in the considered range can be seen in Fig. 12. Here the overall scatter of delay times for all the combinations – eight in total – in the source time parameters are displayed. The coherence in these examples did, in no case, suffer from the different source time functions. Thus, in practice this kind of error would be hard to detect. The absolute amount of spurious delay times easily reached the sampling interval (3.75 ms) in the present analysis.

C) The influence of additive noise

White noise was added to the seismograms presented in Fig. 11 in order to investigate the influence of noise. The results are given in Fig. 13. As can be seen from Fig. 13c in comparison with Fig. 11c, for regions were the signal-to-noise ratio is high, the delay times are not affected by additive noise. This agrees well with Ito's assumption (Ito, 1985).

Discussion and conclusions

Cross spectral analysis methods provide a powerful tool for a precise measurement of differential times between similar earthquakes. For the Swabian Jura seismic network, due to the precision of the internal clock synchronization, the maximum timing accuracy is limited to approximately 1 ms.

In terms of relocation precision, this corresponds to approximately 5 m. This offers an exciting possibility for high-resolution relative hypocentral determinations and the study of the fine structure of source regions (Ito, 1985). Prerequisite, however, are small original spatial differences for the events to be compared. The scatter of the delay times for the individual components increases strongly for the Swabian Jura earthquakes recorded from source locations further apart than 1.5 km. In these cases, *S*-wave delay times averaged over the individual components might, therefore, not be representative of the actual delay times. This effect can be understood from the observation geome-

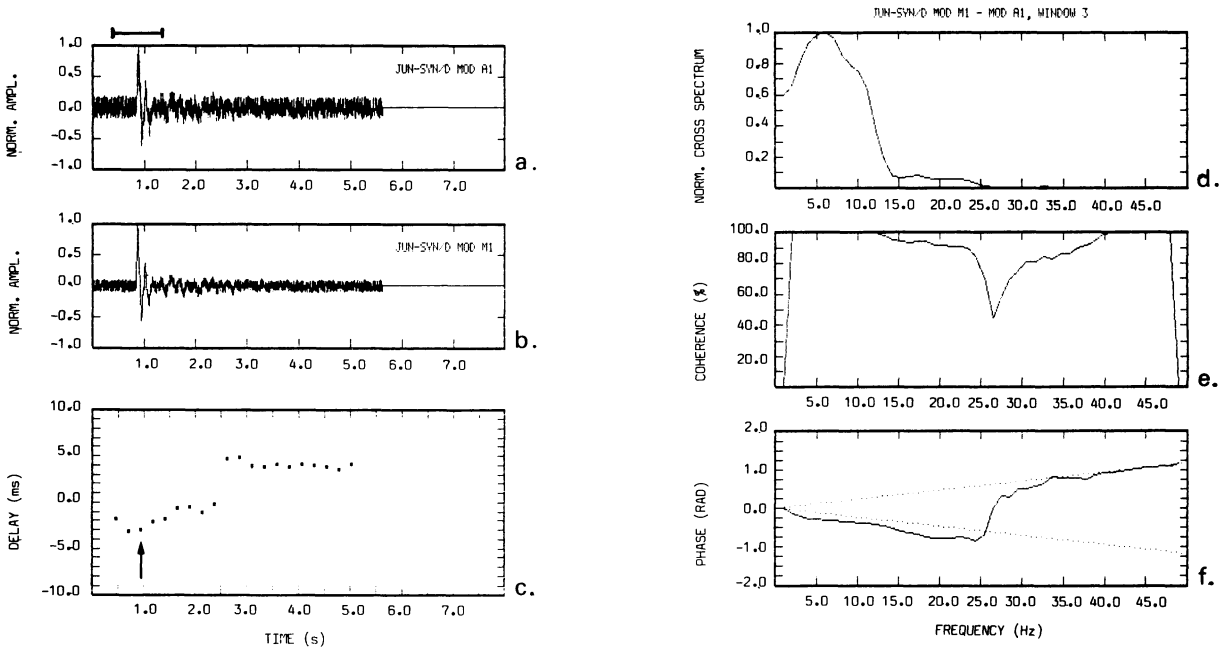

Fig. 13a–f. Cross spectral analysis of noisy synthetic seismograms. The seismograms are the same as in Fig. 11. **a** and **b** show the aligned *SH* seismograms, **c** gives the differential times versus lapse time. **d** shows the cross amplitude spectrum for the window containing the *S* pulses. **e** and **f** give the corresponding coherence and cross phase spectrum, respectively. The *dotted line* in the phase plot corresponds to the delay time equal to the sampling interval

try. Due to different back azimuths, the two events to be compared are observed in apparently different coordinate systems. With simultaneously sampled three-component records, this effect could possibly be reduced by simple coordinate rotation. In this context, multiplexed analog to digital conversion, as used in the Swabian Jura seismic network, shows severe disadvantages.

From the analysis of synthetic seismogram data, the influence of additive, uncorrelated white noise seems to be negligible as long as the signal/noise ratio is high, approximately >4–5 in the considered cases.

No evidence for velocity variations in the Swabian Jura area could be detected from the present analysis. Provided two earthquakes were generated at the same location, a prerequisite for the applicability of the CSA method to monitor velocity variations is the equality of the shape of the source signal. Any differences in the phase spectra of the sources, which do not necessarily have to be a linear function of frequency, are subject to the regression analysis and will be treated as delay time differences. Even changes which do not show up significantly in the coherence (cf. Fig. 11c) might spuriously introduce delay times of the order of the digitization interval. Thus, the coherence spectrum does not seem to be a sufficient measure to detect source time function differences, which might spoil a velocity monitoring analysis using CSA.

For the purpose of relative localization, the influence of source shape differences might not be as severe in special cases, provided that directivity effects at the source are negligible. If the phase shift introduced from the source is identical in all azimuths and incidence angles, the relative location will be correct and the time delay will be considered only as an origin time difference.

In order to investigate these effects more thoroughly, the influence of complex sources producing anisotropic phase changes and their influence on the relocalization should to be modelled. This is, however, beyond the scope of this paper. Additionally, the observation of quarry blast signals, where differences in the source signals could actually be observed, would be of great interest. However, no adequate data for the Swabian Jura seismic network were at our disposal.

Acknowledgements. The comments of the reviewers are greatly appreciated.

References

Dewey, J.W: A consumer's guide to instrumental methods for determination of hypocenters. Geol. Soc. Am., Rev. in Eng. Geol. **IV**, 109–117, 1979

Evernden, J.F.: Identification of earthquakes and explosions by use of teleseismic data. J. Geophys. Res. **74**, 3828–3856, 1969

Frechet, J.: Sismogenese et doublets sismiques. Ph. D. thesis, University of Grenoble, 206 pp., 1985

Fremont, M.J.: Mesure de variations temporelles des paramètres de la croûte terrestre et d'effets de sources par traitement de doublets de séismes. Ph. D. thesis, University of Grenoble, 220 pp., 1984

Gelbke, C.: Erweiterung des Erdbebenlokalisierungsprogramms HYPO71 (Lee and Lahr, 1972) um eine Laufzeitroutine fuer Mehrschichtenmodelle konstanter positiver und negativer Geschwindigkeitsgradienten. Geophys. Inst. Univ. Karlsruhe, 58 pp., 1977

Haessler, H., Hoang-Trong, P., Schick, R., Schneider, G., Strobeck, K.: The September 3, 1978, Swabian Jura earthquake. Tectonophysics **68**, 1–14, 1980

Haskell, N.A.: Crustal reflection of plane SH waves. J. Geophys. Res. **65**, 4147–4150, 1960

Ito, A.: High resolution relative hypocenters of similar earthquakes by cross-spectral analysis method. J. Phys. Earth **33**, 279–294, 1985

Kanasewich, E.R.: Time sequence analysis in geophysics. The University of Alberta Press, 480 pp., 1981

Langer, H.: Seismotektonische Herdparameter und Ausbreitungseffekte bei Mikroerdbeben im Bereich der westlichen Schwaebischen Alb. Ph. D. thesis, University of Stuttgart, 113 pp., 1986

Lee, W.H.K., Lahr, L.C.: HYPO71: A computer program for determining hypocenter, magnitude and first motion pattern of local earthquakes. U. S. Geol. Survey, Open File Report, 113 pp., 1972

Poupinet, G., Ellsworth, W.L., Frechet, J.: Monitoring velocity variations in the crust using earthquake doublets: An application to the Calaveras Fault, California. J. Geophys. Res. **89**, 5719–5731, 1984

Poupinet, G., Frechet, J., Ellsworth, W.L., Fremont, M.J., Glangeaud, F.: Doublet analysis: Improved accuracy for earthquake prediction studies. Earthq. Predict. Res. **3**, 147–159, 1985

Scherbaum, F.: Die seimische Erkundung des Stationsuntergrundes mit Nahbebenseismogrammen. Habilitation thesis, University of Stuttgart, 209 pp., 1986

Scherbaum, F., Stoll, D.: Source parameters and scaling laws of the 1978 Swabian Jura (Southwest Germany) aftershocks. Bull. Seismol. Soc. Am. **73**, 1321–1343, 1983

Scherbaum, F., Stoll, D.: The estimation of Green's function from local earthquake recordings and the modelling of the site response. Phys. Earth Planet. Inter. **38**, 189–202, 1985

Turnovsky, J., Schneider G.: The seismotectonic character of the September 3, 1978, Swabian Jura earthquake series. Tectonophysics **83**, 151–162, 1982

Received May 28, 1986; revised version September 8, 1986
Accepted September 19, 1986